ChemSusChem

Supporting Information

Investigation of SnS_2-rGO Sandwich Structures as Negative Electrode for Sodium-Ion and Potassium-Ion Batteries

Chengping Li, Kristina Pfeifer, Xianlin Luo, Georgian Melinte, Jinsong Wang, Zhengfu Zhang,* Yingjie Zhang, Peng Dong, Angelina Sarapulova, Helmut Ehrenberg, and Sonia Dsoke*

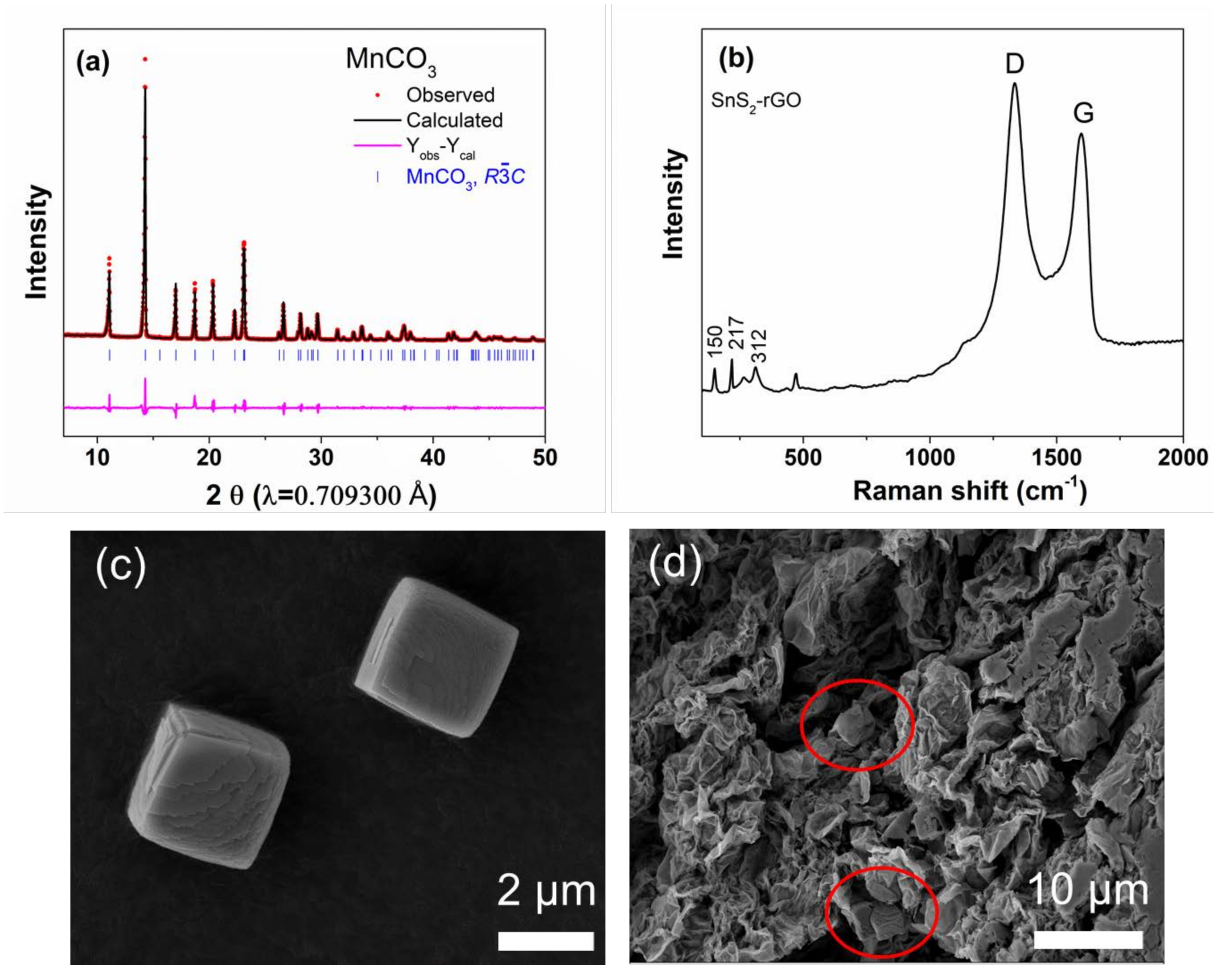

Figure S1. XRD patterns of the $MnCO_3$ microcubes template (a); Raman spectra of the SnS_2-rGO composites (b); SEM images of the $MnCO_3$ microcubes template (c) and $MnCO_3$@SnS_2-rGO (d).

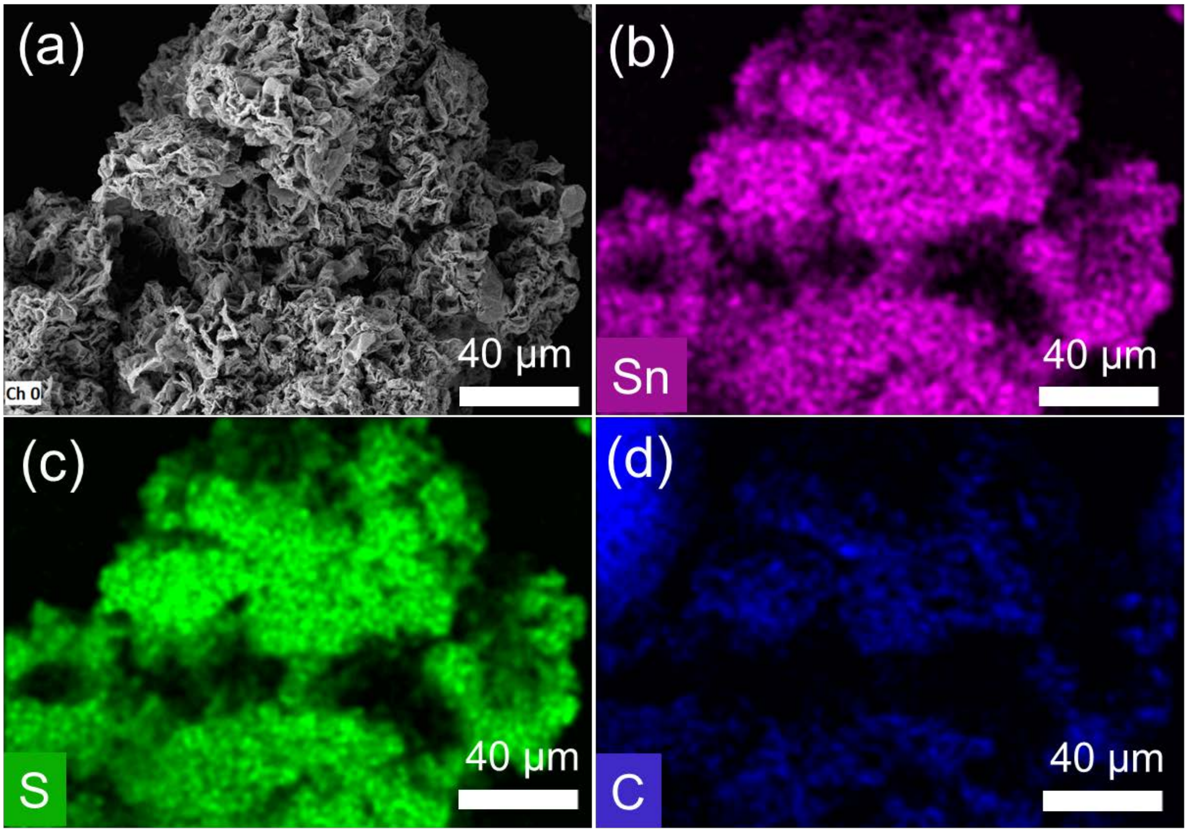

Figure S2. SEM image (a) and EDX elemental mapping of elemental (b) Sn, (c) S, and (d) C.

Table. S1 Organic Elemental Analysis (OEA) of the pristine SnS_2-rGO material

	N (%)	C (%)	H (%)	S (%)
SnS_2-rGO	0.2	15.6	0.8	28.1

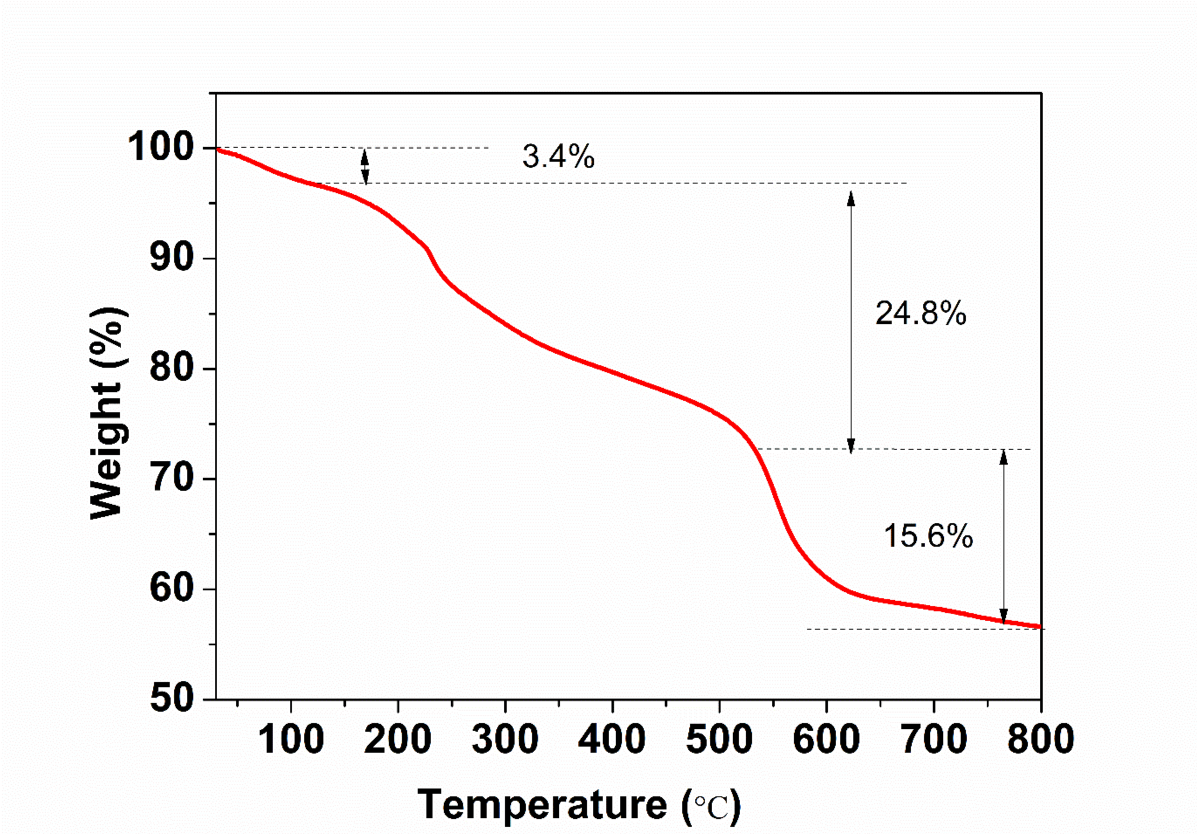

Figure S3. TGA curve of the SnS_2-rGO composite.

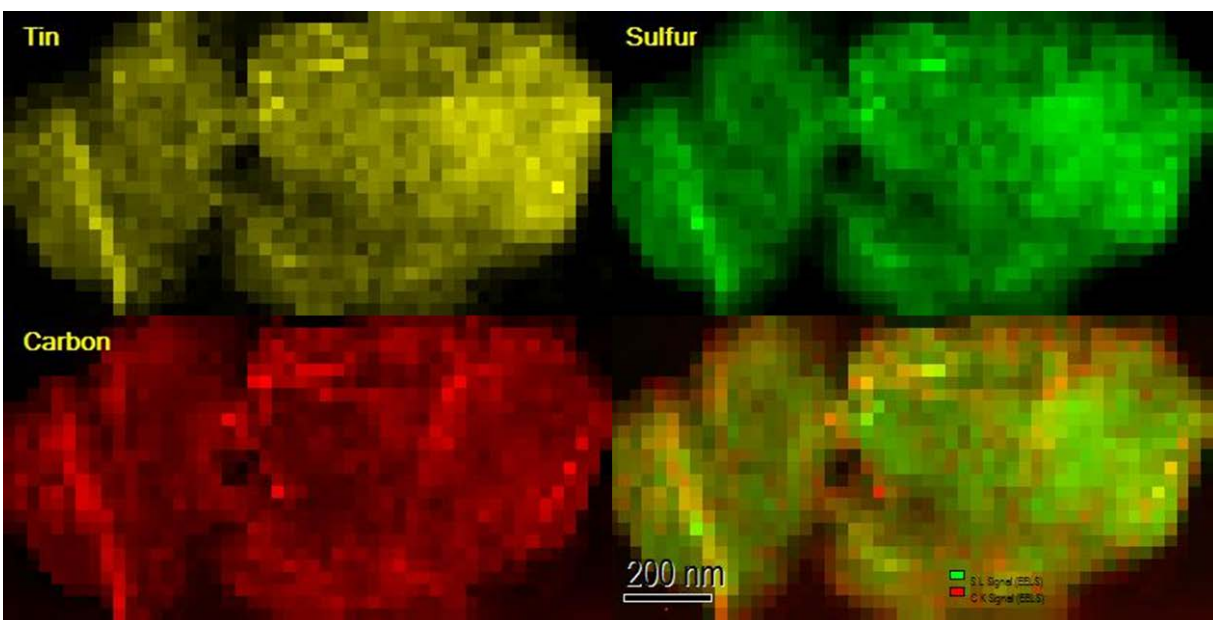

Figure S4. Electron energy loss spectroscopy (EELS) mapping of the SnS_2-rGO.

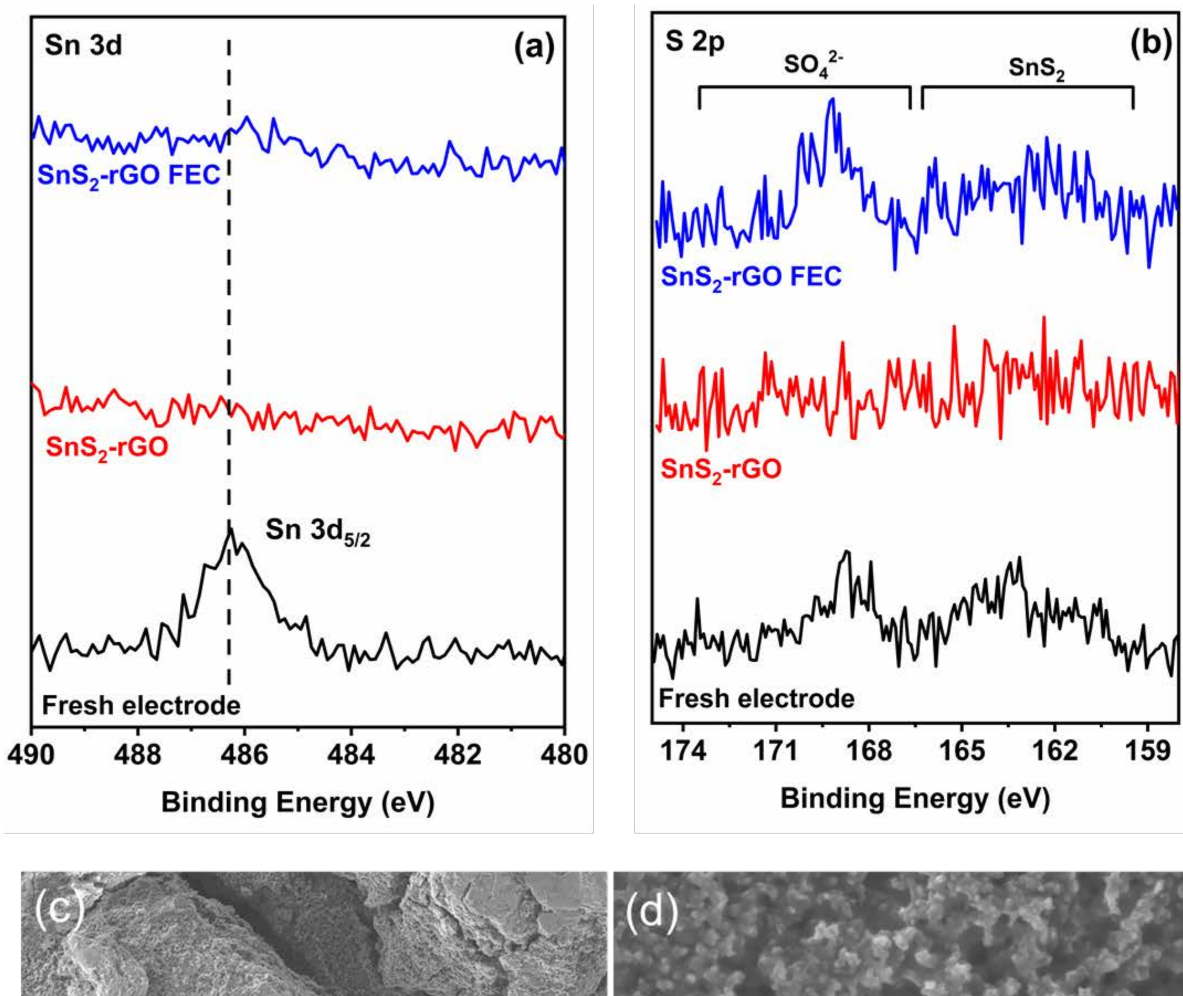

Sn 3d
(a)
SnS2-rGO FEC
SnS2-rGO
Sn 3d5/2
Fresh electrode
490
488
486
484
482
480
Binding Energy (eV)
S 2p
(b)
SO4 2-
SnS2
SnS2-rGO FEC
SnS2-rGO
Fresh electrode
174
171
168
165
162
159
Binding Energy (eV)
(c)
10 μm
20th cycle
(d)
200 nm
20th cycle
(e)
10 μm
20th cycle + FEC
(f)
200 nm
20th cycle + FEC

Figure S5. Effect of FEC on electrochemical performances**:** long-term cycling and CE of the SnS_2-rGO electrode with Super P carbon additive at a specific current of 0.2 A g^{-1} (a); galvanostatic sodiation/de-sodiation capacity profiles at some selective cycles (b); SEM images of the SnS_2-rGO electrode after 20 cycles in the FEC free electrolyte (c, d) and 5 wt% FEC-containing electrolytes (e, f), respectively.

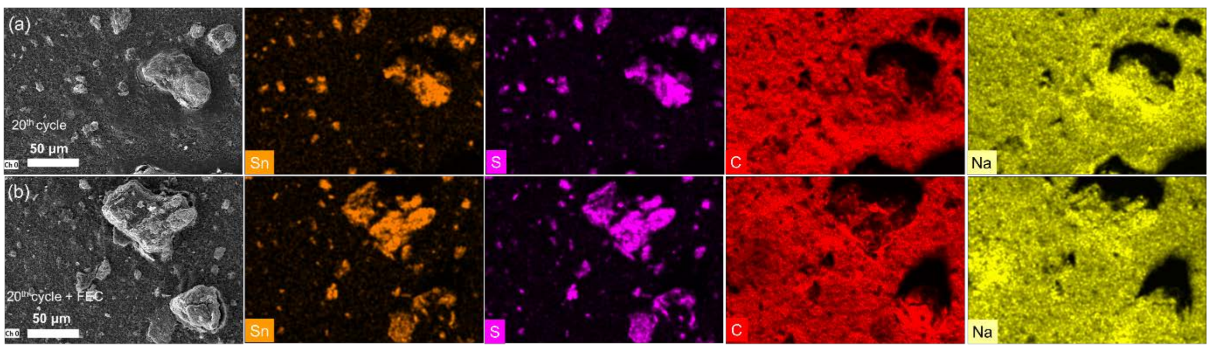

Figure S6. EDS elemental mapping of the SnS_2-rGO (Super P) electrode after 20 cycles in the FEC free electrolyte (a) and 5 wt% FEC-containing electrolytes (b), respectively.

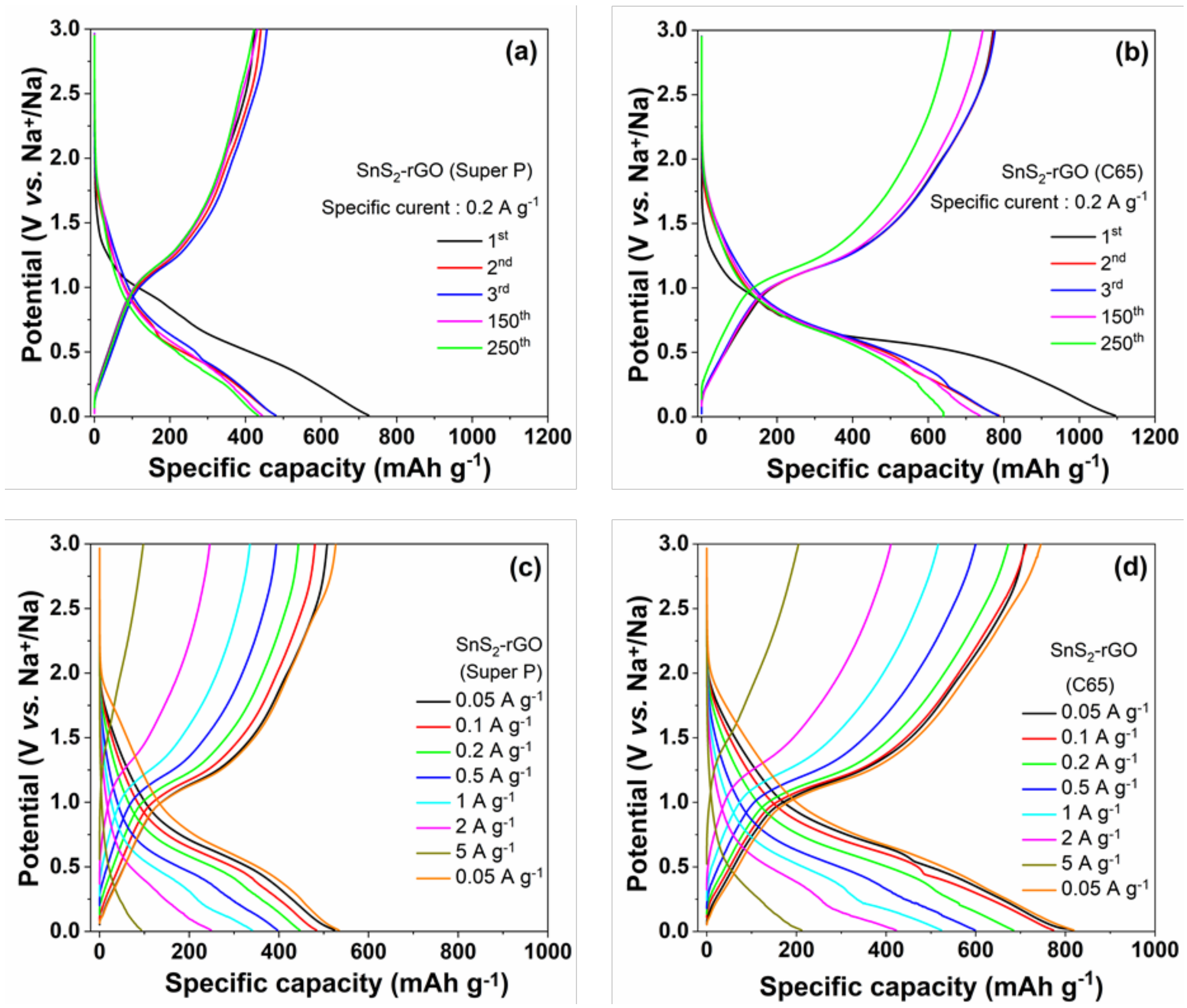

Figure S7. Galvanostatic sodiation/de-sodiation capacity profiles at some selective cycles with Super P (a) and C65 conductivity (b); sodiation and de-sodiation capacity curves with Super P (c) and C65 conductivity (d) at different specific currents.

Table S2. Summary of the Sn-based sulfides electrodes materials for NIBs applications

Electrode material	Carbon additive	Potential (V)	First sodiation capacity (mAh g^{-1} (A g^{-1}))	Capacity after (x) cycles (mAh g^{-1})	CE in the first cycle	Capacity at high rate (mAh g^{-1} (A g^{-1}))	additive	Ref.
layered SnS_2-on RGO	Acetylene black	0.01−2.5	630(0.2)	628 (100)	75%	610(0.5); 590(1) ; 544(2)	NA	[1]
exfoliated SnS_2 on graphene	Super P	0.01−2.5	864.5(0.2)	610(100)	69%	532(0.5); 461(1); 381 (2); 326(4)	CMC	[2]
3D SnS_2/rGO	Acetylene black	0.01−2.5	754(0.1)	401(700)	78%	663(0.5); 608(1); 449(5)	CMC FEC	[3]
2D SnS_2/CNTs	Super P	0.01-2.5	1063(0.05)	476(100)	46.7%	396(0.8); 341(1.6); 265(3.2);	PVDF FEC	[4]
SnS_2-RGO	Acetylene black	0.01-2.5	630(0.2)	628(100)	75%	552(0.2); 500 (0.4)	CMC	[1]
SnS_2–NGS	carbon black	0.01-3.0	900(0.2)	450(100)	64%	430(1); 342(2); 232(5)	FEC	[5]

SnS_2/Graphene-CNT	Super P	0.005-3.0	930(0.2)	535（100）	50%	430(1); 342(2); 304.8(10)	FEC	[6]
SnS_2-rGO	Super P	0.01-3.0	726(0.2)	420(250)	58.5%	390(1); 339(2); 207(5)	CMC FEC	This work
SnS_2-rGO	C65	0.01-3.0	1094(0.2)	635(250)	70.5%	522(1); 424(2); 210(5)	CMC FEC	

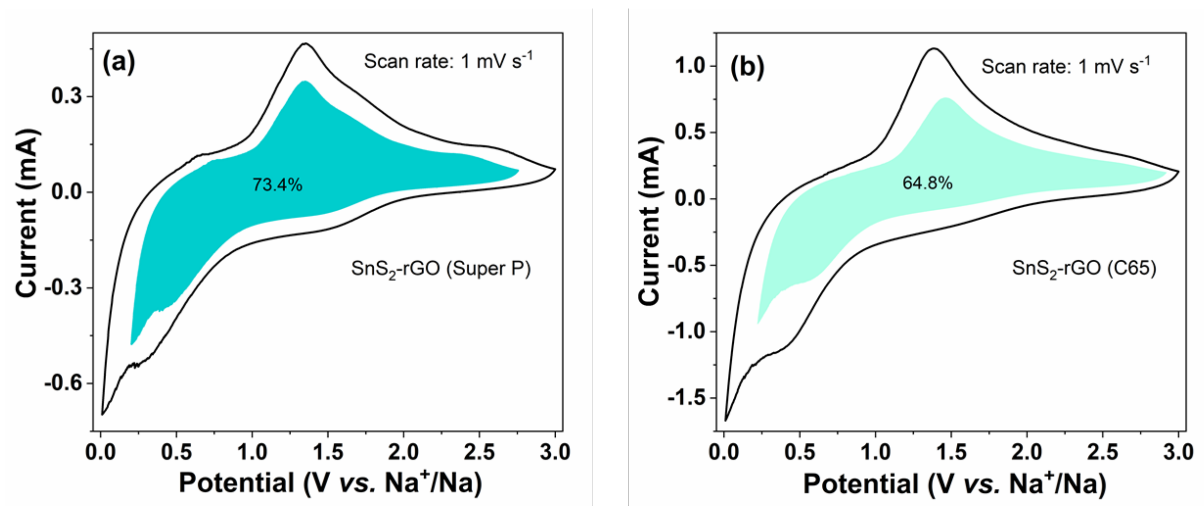

Figure S8. CV plots with the pseudo-capacitive contribution shown by the shadow region at a scan rate of 1 mV s^{-1} of SnS_2-rGO with Super P (a) and C65 (b).

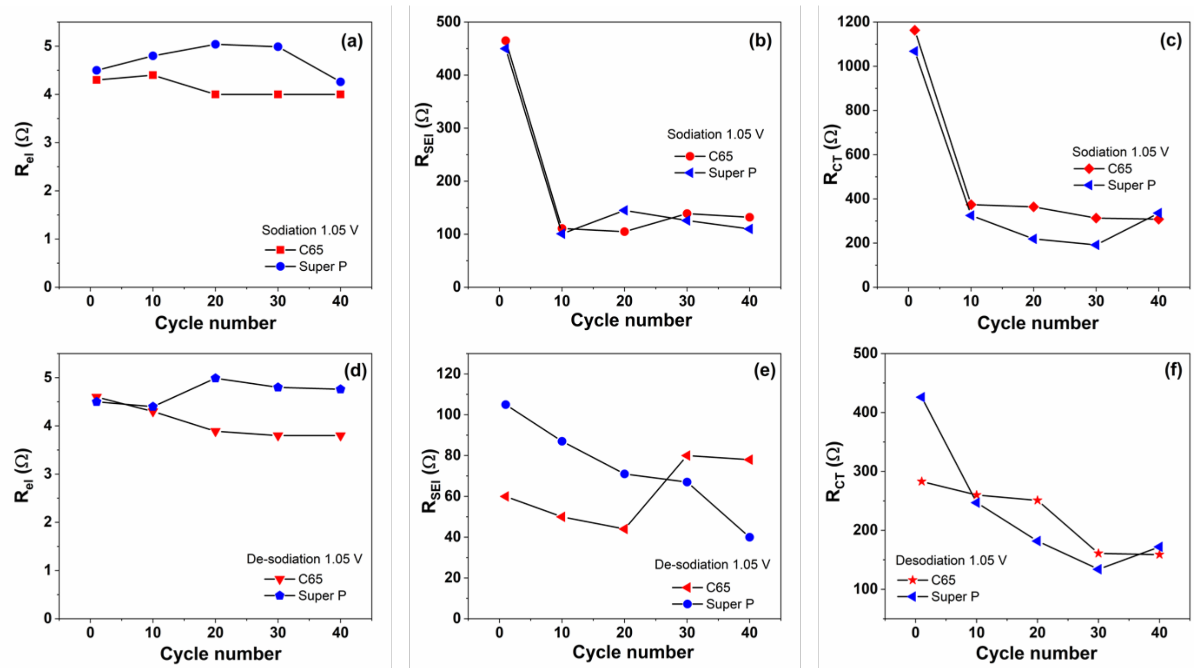

Figure S9. Resistance values for SnS_2-rGO electrode with Super P and C65 in sodiation condition: R_{el} (a), R_{SEI} (b), R_{CT} (c); in de-sodiation condition: R_{el} (d), R_{SEI} (e), and R_{CT} (f).

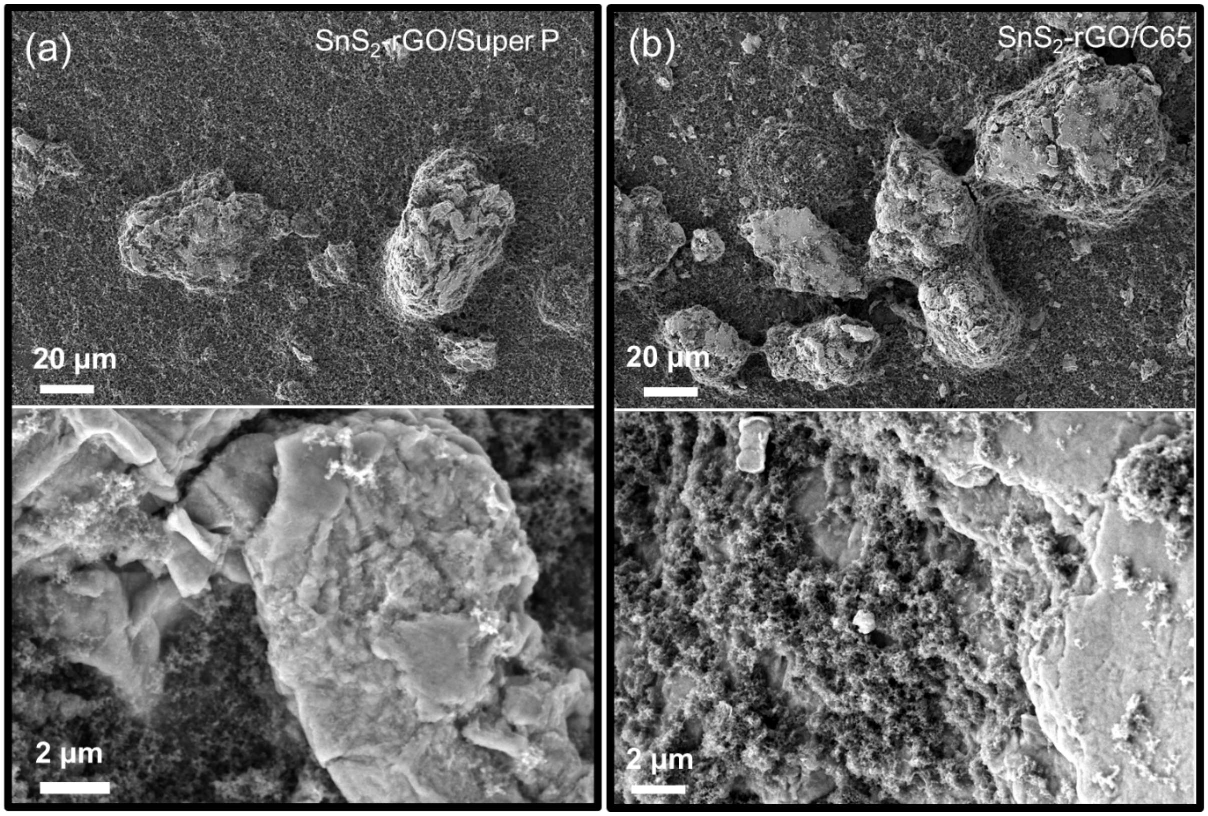

Figure S10. SEM images of the fresh SnS_2-rGO electrode with Super P carbon additive (a) and C65 conductive additive (b).

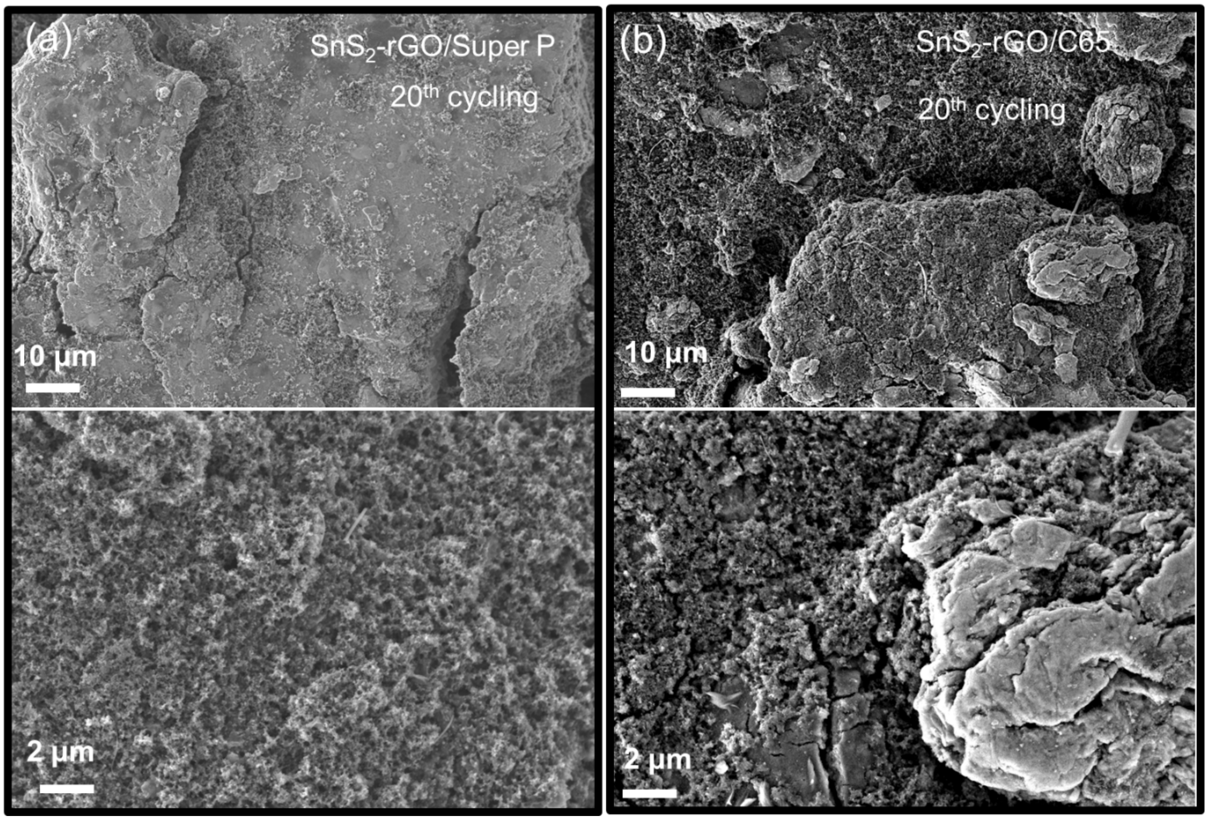

Figure S11. SEM images of the SnS_2-rGO electrode with Super P carbon additive (a) and C65 conductive additive (b) after 20 cycles in SIBs.

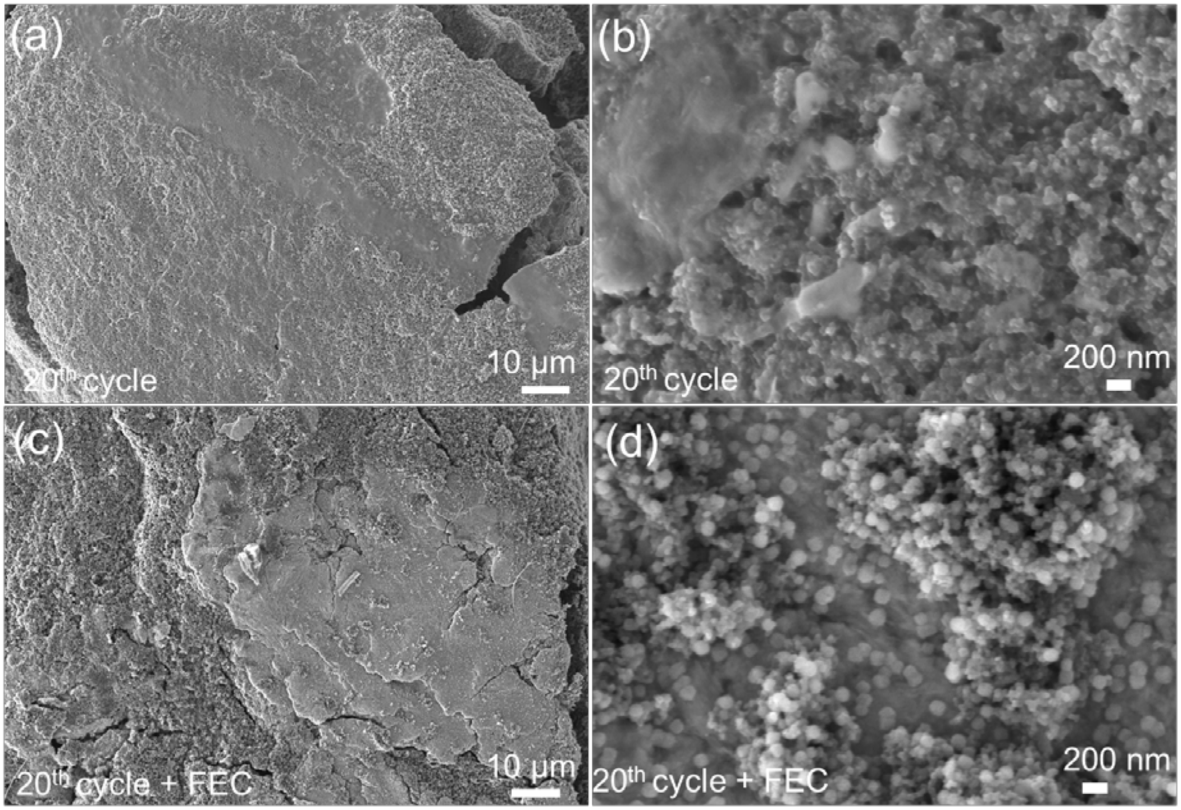

Figure S12. SEM images of the SnS_2-rGO (Super P) electrode in the FEC free electrolyte (a, b) and 5 wt% FEC-containing electrolytes (c, d) after 20 cycles.

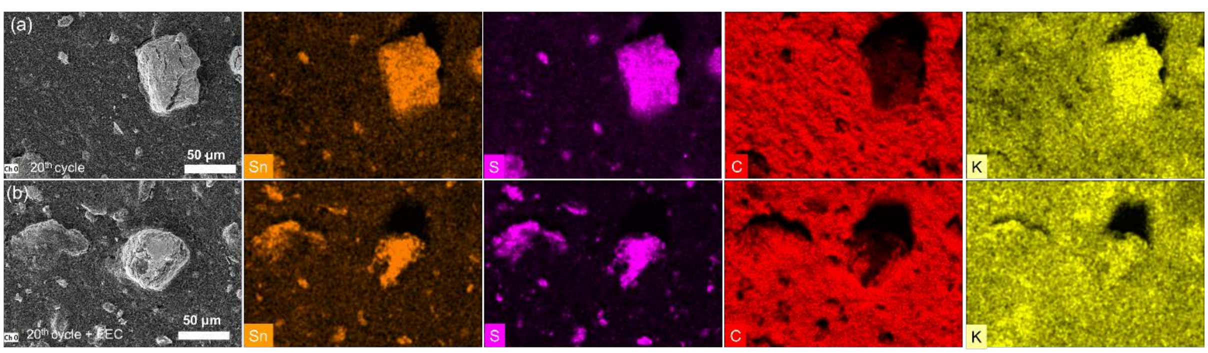

Figure S13. EDS elemental mapping of the SnS_2-rGO (Super P) electrode in the FEC free electrolyte (a) and 5 wt% FEC-containing electrolytes (b) after 20 cycles.

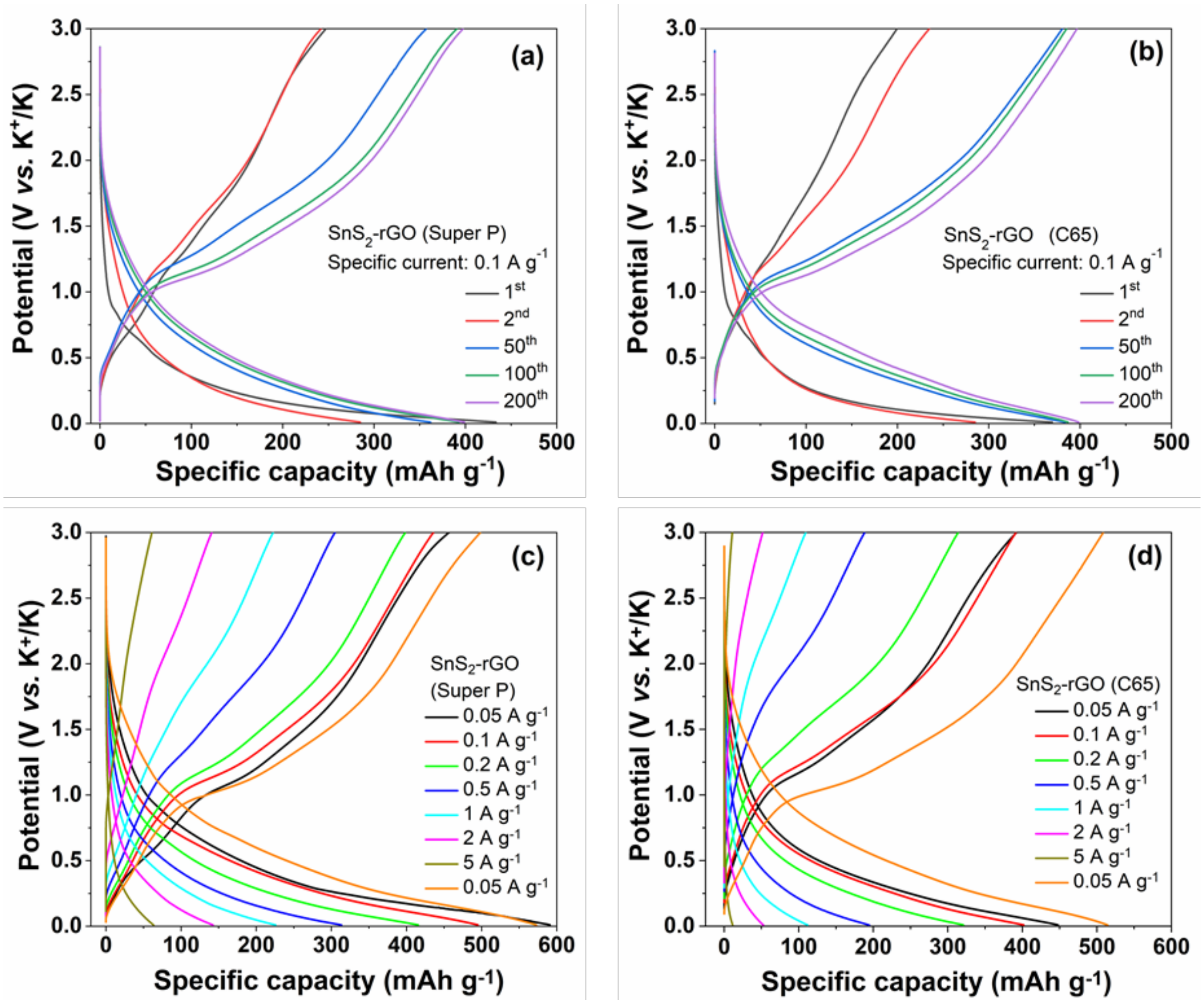

Figure S14. Galvanostatic potassiation/de-potassiation capacity curves at some chosen cycles with Super P (a) and C65 (b); potassiation and de-potassiation capacity curves with Super P (c) and C65 (d) at various specific currents.

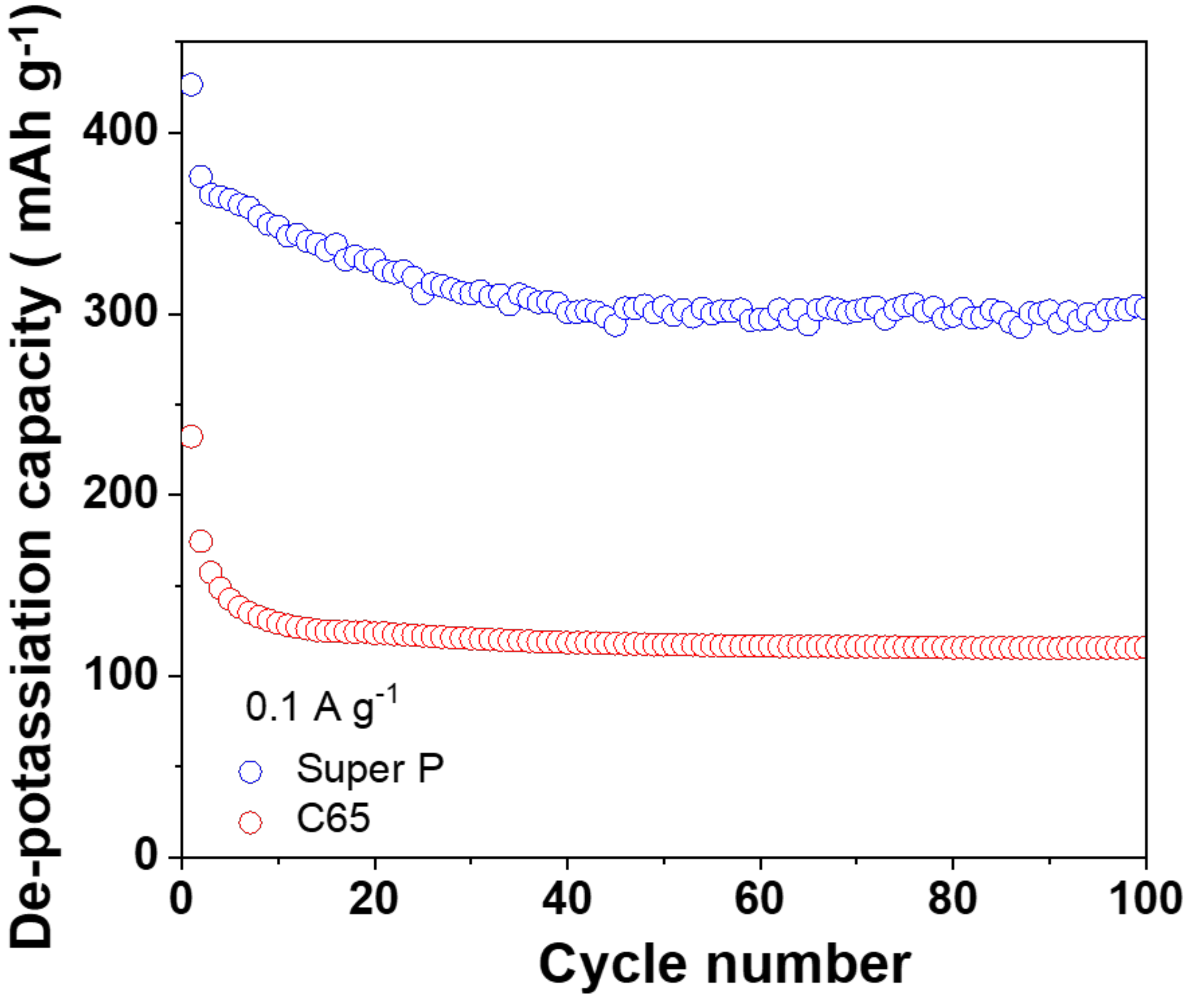

Figure S15. Long-term cycling performance of Super P and C65 electrode at a specific current of 0.1 A g^{-1} in KIBs.

Table S3. Summary of the Sn-based sulfides electrodes materials for KIBs applications.

Electrode material	Carbon additive	Potential (V)	First potassiation capacity (mAh g^{-1} (A g^{-1}))	Capacity after (x) cycles (mAh g^{-1})	CE in the first cycle	Capacity at high rate (mAh g^{-1} (A g^{-1}))	additive	Ref.
SnS_2@rGO nanosheets	Super P	0.01−2.0	819(0.05)	387 (100)	51.2%	355(0.2); 289(0.5); 247(1)	FEC	[7]
SnS_2@C@rGO	Super P	0.01−3.0	499(0.05)	309 (100)	53%	346(0.3); 312(0.4); 288 (0.5)	FEC	[8]
SnS_2-RGO	Super P	0.01−2.0	630(0.025)	300(30)	56%	120(2)	CMC	[9]
SnS_2-RGO	Super P	0.01-3.0	650(0.1)	436(50)	69%	311(0.5)	PVDF	[10]
SnS_2@NC	carbon black	0.01-3.0	1510(0.05)	262(100)	38.4%	363.5(0.4); 237 (0.8); 206.7 (1)	NA	[11]
flake-SnS_2	Super P	0.25-2.35	810(0.1)	312(30)	56.5%	135(0.5); 112 (0.8)	CMC	[12]
SnS_2/RGO	Super P	0.01-3.0	983(0.05)	130（300）	53%	281(0.5)	NA	[13]

SnS_2-rGO	Super P	0.01-3.0	433(0.1)	420(250)	57%	225(1); 142(2);63(5)	CMC FEC	This work
SnS_2-rGO	C65	0.01-3.0	369(0.1)	635(250)	54%	112(1); 52(2); 11(5)	CMC	

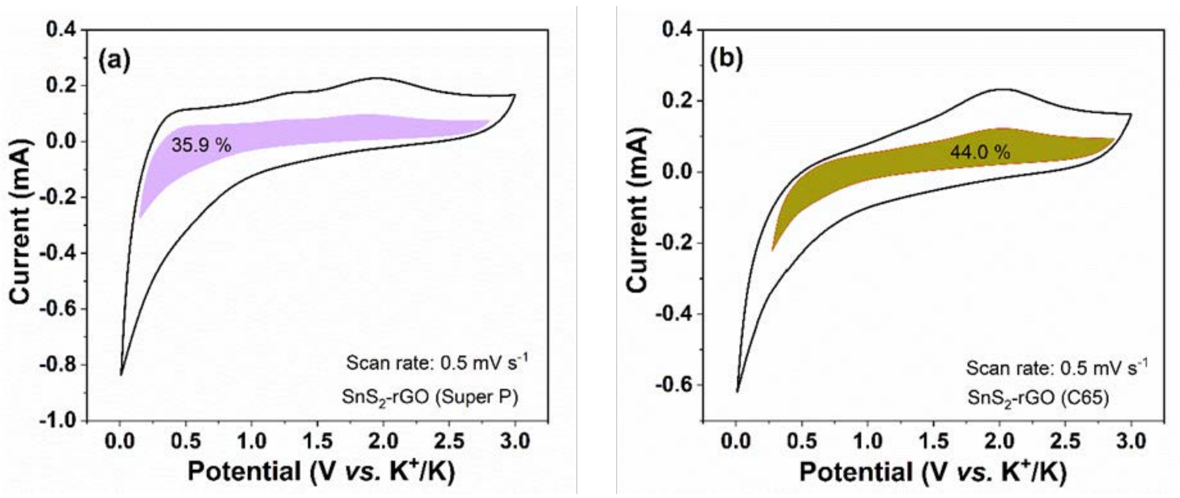

Figure S16. CV plots with the pseudocapacitive contribution are shown by the shadow region at a scan rate of 1 mV s^{-1} of SnS_2-rGO with Super P (c) and C65 (d).

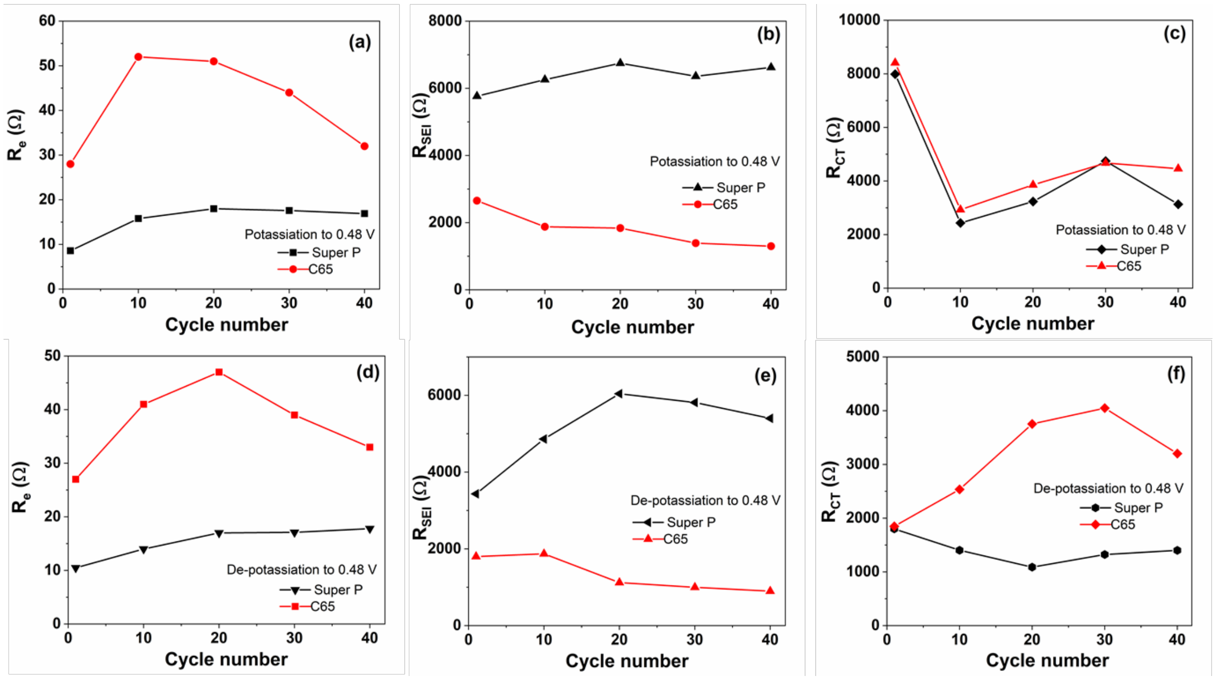

Figure S17. Resistance values for SnS_2-rGO electrode with Super P and C65 in potassiation condition: R_e (a), R_{SEI} (b), R_{CT} (c); in de-potassiation states: R_e (d), R_{SEI} (e), and R_{CT} (f).

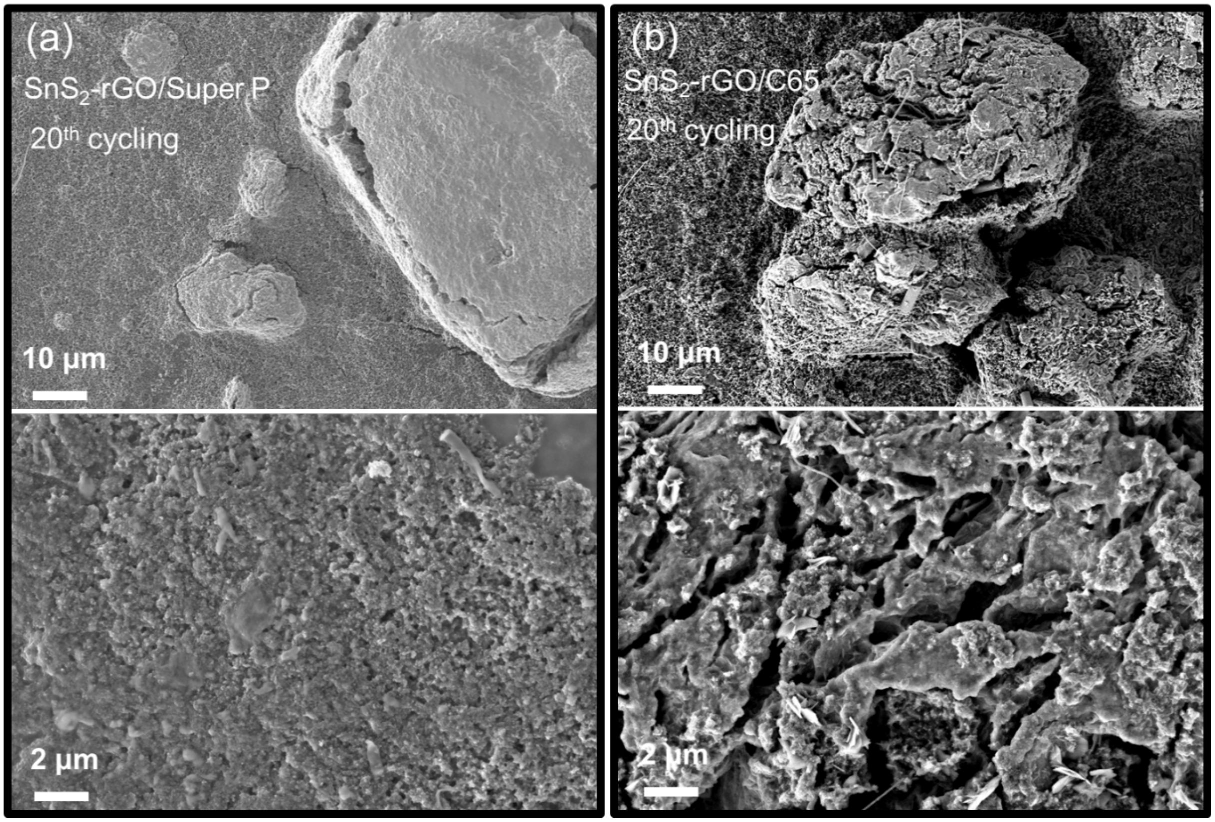

Figure S18. SEM images of the SnS_2-rGO electrode with Super P (a) and C65 conductive additive (b) after 20 cycles in KIBs.

Reference

[1] B. Qu, C. Ma, G. Ji, C. Xu, J. Xu, Y. S. Meng, T. Wang, J. Y. Lee, *Advanced Materials* **2014**, *26*, 3854–3859.

[2] Y. Liu, H. Kang, L. Jiao, C. Chen, K. Cao, Y. Wang, H. Yuan, *Nanoscale* **2015**, *7*, 1325–1332.

[3] J. Zheng, X. Xiong, G. Wang, Z. Lin, X. Ou, C. Yang, M. Liu, *Chemical Engineering Journal* **2018**, *339*, 78–84.

[4] S. Zhang, H. Zhao, M. Wu, L. Yue, J. Mi, *Journal of Alloys and Compounds* **2018**, *737*, 92–98.

[5] Y. Jiang, Y. Feng, B. Xi, S. Kai, K. Mi, J. Feng, J. Zhang, S. Xiong, *Journal of Materials Chemistry A* **2016**, *4*, 10719–10726.

[6] J. Cui, S. Yao, Z. Lu, J.-Q. Huang, W. G. Chong, F. Ciucci, J.-K. Kim, *Advanced Energy Materials* **2018**, *8*, 1702488.

[7] L. Fang, J. Xu, S. Sun, B. Lin, Q. Guo, D. Luo, H. Xia, *Small* **2019**, 1804806.

[8] D. Li, Q. Sun, Y. Zhang, L. Chen, Z. Wang, Z. Liang, P. Si, L. Ci, *ChemSusChem* **2019**, *12*, 2689–2700.

[9] V. Lakshmi, Y. Chen, A. A. Mikhaylov, A. G. Medvedev, I. Sultana, M. M. Rahman, O. Lev, P. V. Prikhodchenko, A. M. Glushenkov, *Chemical Communications* **2017**, *53*, 8272–8275.

[10] J. Xie, Y. Zhu, N. Zhuang, X. Li, X. Yuan, J. Li, G. Hong, W. Mai, *Journal of Materials Chemistry A* **2019**, *7*, 19332–19341.

[11] L. Cao, B. Zhang, X. Ou, C. Wang, C. Peng, J. Zhang, *ChemElectroChem* **2019**, *6*, 2254–2263.

[12] R. Hu, Y. Fang, X. Liu, K. Zhu, D. Cao, J. Yi, G. Wang, *Chemical Research in Chinese Universities* **2021**, *37*, 311–317.

[13] L. Wu, H. Shao, C. Yang, X. Feng, L. Han, Y. Zhou, W. Du, X. Sun, Z. Xu, X. Zhang, F. Jiang, C. Dong, *Nanomaterials* **2021**, *11*, 1932.